Physics in High Magnetic Fields / Physique en champ magnétique intense

Graphene in high magnetic fields

Graphène sous champ magnétique intense

Milan Orlita [a,c], Walter Escoffier [b], Paulina Plochocka [b], Bertrand Raquet [b], Uli Zeitler [d,*]

[a] *Laboratoire national des champs magnétiques intenses, CNRS-UJF-UPS-INSA, 38042 Grenoble cedex 9, France*
[b] *Laboratoire national des champs magnétiques intenses, CNRS-UJF-UPS-INSA, 143, avenue de Rangueil, 31400 Toulouse, France*
[c] *Institute of Physics, Faculty of Mathematics and Physics, Charles University, Ke Karlovu 5, 121 16 Praha 2, Czech Republic*
[d] *Radboud University Nijmegen, High Field Magnet Laboratory and Institute for Molecules and Materials, Toernooiveld 7, 6525 ED Nijmegen, The Netherlands*

A R T I C L E   I N F O

A B S T R A C T

Carbon-based nano-materials, such as graphene and carbon nanotubes, represent a fascinating research area aiming at exploring their remarkable physical and electronic properties. These materials not only constitute a playground for physicists, they are also very promising for practical applications and are envisioned as elementary bricks of the future of the nano-electronics. As for graphene, its potential already lies in the domain of opto-electronics where its unique electronic and optical properties can be fully exploited. Indeed, recent technological advances have demonstrated its effectiveness in the fabrication of solar cells and ultra-fast lasers, as well as touch-screens and sensitive photo-detectors. Although the photo-voltaic technology is now dominated by silicon-based devices, the use of graphene could very well provide higher efficiency. However, before the applied research to take place, one must first demonstrates the operativeness of carbon-based nano-materials, and this is where the fundamental research comes into play. In this context, the use of magnetic field has been proven extremely useful for addressing their fundamental properties as it provides an external and adjustable parameter which drastically modifies their electronic band structure. In order to induce some significant changes, very high magnetic fields are required and can be provided using both DC and pulsed technology, depending of the experimental constraints. In this article, we review some of the challenging experiments on single nano-objects performed in high magnetic and low temperature. We shall mainly focus on the high-field magneto-optical and magneto-transport experiments which provided comprehensive understanding of the peculiar Landau level quantization of the Dirac-type charge carriers in graphene and thin graphite.

© 2012 Académie des sciences. Published by Elsevier Masson SAS. All rights reserved.

R É S U M É

Les nano-matériaux à base de carbone, tels que le graphène et les nanotubes de carbone, représentent un domaine de recherche fascinant dédié à l'exploration de leurs propriétés physiques et électroniques remarquables. Ces matériaux ne sont pas que des curiosités pour les physiciens, ils sont aussi très prometteurs pour des applications pratiques et ont même été suggérés comme composants élémentaires de l'électronique du futur. Dans le cas du graphène, son potentiel est déjà exploité dans le domaine de l'opto-électronique.

* Corresponding author.
  E-mail addresses: milan.orlita@lncmi.cnrs.fr (M. Orlita), walter.escoffier@lncmi.cnrs.fr (W. Escoffier), paulina.plochocka@lncmi.cnrs.fr (P. Plochocka), bertrand.raquet@lncmi.cnrs.fr (B. Raquet), u.zeitler@science.ru.nl (U. Zeitler).

En effet, de récentes avancées technologiques ont permis son intégration dans des cellules photo-voltaïques, dans des lasers ultra-rapides, des écrans tactiles ou encore des photo-détecteurs. Bien que la technologie photo-voltaïque soit encore dominée par l'utilisation du silicium, le graphene serait susceptible de le remplacer à terme. Cependant, avant que de telles recherches appliquées ne débutent, il fut nécessaire de découvrir et de démontrer le potentiel des nano-objets à base de carbone, ce qui constitue le rôle de la recherche fondamentale. Dans ce contexte, l'application d'un champ magnétique externe se révèle extrêmement utile afin de sonder leurs propriétés fondamentales car il agit tel un paramètre ajustable qui modifie leurs structures de bande électronique. Afin d'entrevoir ces changements, il est nécessaire d'utiliser des champs magnétiques très intenses, soit continus soit pulsés en fonction des contraintes de l'expérience. Dans cet article, nous passons en revue quelques une des expériences notables réalisées sur des nano-objets uniques et dans des conditions extrêmes de température et de champ magnétique. Nous focaliserons notre discussion sur les réalisations expérimentales de magnéto-optique et de magnéto-transport qui ont permis de mieux caractériser la quantification en niveaux de Landau du spectre énergétique des électrons de Dirac dans le graphène et le graphite aminci.

1. Introduction

The experimental realization of a new material may lead to the emergence of new spectacular physics. Graphene, only realized experimentally less than a decade ago [1] is a prominent example. Indeed, the discovery of graphene opened an entirely new research field [2,3] concerning fundamental physics but also having a tremendous application potential. High-magnetic-field experiments were and are still an important tool to uncover its intriguing properties. For instance, the discovery of a half-integer quantum Hall effect in single-layer graphene [4,5] and an unconventional integer quantum Hall effect in bilayer graphene [6] served as a smoking gun for the existence of massless chiral Dirac fermions in single-layer graphene and relativistic massive charge carriers in bilayer graphene.

High-field experiments on graphene are performed in different magnet labs word wide. For instance, magneto-optical experiments at the National High Magnetic field Laboratory (NHFML) in Tallahasse [7–9] were extremely useful to uncover graphene's Landau level structure. The Landau levels were also investigated by means of magneto-transport experiments at NHMFL [10–13] and at the High Field Magnet Laboratory (HFML) in Nijmegen [6,13–17] and, in particular, it was further possible to unveil the fine structure of the zero-energy level in single-layer and bilayer graphene [10–12,16] to observe a fractional quantum Hall effect [18] and to measure the quantum Hall effect up to room temperature [13].

This article presents an overview of high-field experiments on graphitic systems performed in the last decade at the LNCMI (Laboratoire nationale des champs magnétiques intenses) in Grenoble (DC fields) and Toulouse (pulsed fields). We consider a number of experiments on various graphene-based materials which extended the current carbon physics. The paper starts with an introductory Section 2 where we briefly review the physical properties of graphene, in particular at high magnetic fields. Section 3 will deal specifically with a selection of magneto-optical experiments performed at LNCMI addressing the peculiar Landau level structure of graphite in graphene in high magnetic fields. Finally, Section 4 will cover transport experiments, with an emphasis on pulsed-fields quantum-Hall experiments performed in Toulouse.

2. Theoretical background

The band structure of single-layer graphene has been calculated already in 1947 [19]. Using a tight-binding model Wallace showed that graphene is a zero-gap semiconductor with the conduction and valence bands touching at the K points of the Brillouin zone. Around these points, the dispersion relation of the carriers is nearly linear, $E = \pm v_F p$, mimicking chiral massless Dirac fermions, see Fig. 1(a). The chirality, an additional topological degree of freedom analogous to the spin of real relativistic particles, results from the two triangular sublattices of honeycomb lattice and the energy-independent particle velocity, $v_F \approx 10^6$ m s^{-1}, is directly proportional to the strength of coupling between neighboring carbon atoms.

When stacking two layers of graphene on top of each other, the energetically most favorable form is the AB stacking (often referred to as Bernal stacking), when only one of two triangular sublattices (A or B sublattice) in one layer is directly stacked with the carbon atoms in the other graphene sheet. In this so-called bilayer graphene (BLG), it is just the inter-layer coupling (quantified by the parameter γ_1) which implies a hyperbolic [20] instead of the linear dispersion relation in graphene, see Fig. 1(b): $E(p) = \pm\frac{1}{2}\gamma_1 \pm (\frac{1}{4}\gamma_1^2 + v_F^2\hbar^2 p^2)^{1/2}$, which corresponds to massive, chiral and ultra-relativistic particles. These resemble, at low energies ($|E| \ll \gamma_1$), charge carriers in conventional semiconductors, which are characterized by a parabolic dispersion $E(p) = p^2/2m^*$, with an effective mass of $m^* = \gamma_1/2v_F^2 \approx 0.032m_e$.

The peculiar band structures of graphene mono-layer and bilayer translate at sufficiently high magnetic field into specific Landau level (LL) spectra. In contrast to conventional systems, these levels are no longer equidistant, see Figs. 1(c) and 1(d), and their energies read:
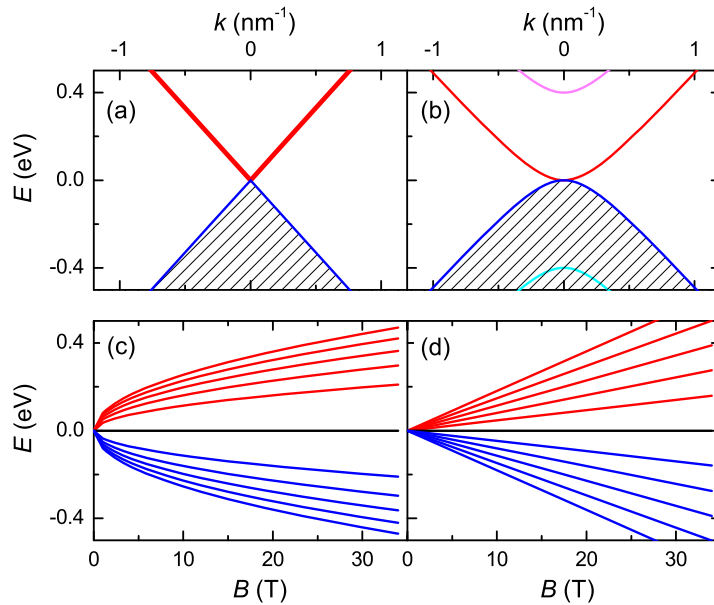
Fig. 1. Dispersion of single-layer graphene (a) and bilayer graphene (b) around the K-point. The shaded regions sketch the occupied states for an undoped system. The bottom panels show the Landau level spectrum for single-layer graphene (c) and bilayer graphene (d).

$$E_N^{\text{SLG}} = \text{sgn}(N)\sqrt{2\hbar v_F^2 eB|N|} \quad \text{and} \quad E_N^{\text{BLG}} = \text{sgn}(N)\frac{\hbar eB}{m^*}\sqrt{|N|(|N|-1)} \tag{1}$$

for SLG [21] and BLG [20,6], respectively. In both cases, N is a negative integer for holes and positive for electrons. Cyclotron resonance experiments performed, amongst other also in LNCMI Grenoble, have indeed confirmed such relativistic-like Landau level spectra [22,7], they will be discussed in detail in Section 3.

A direct consequence of the chiral particles in graphene is the existence of a Landau level at zero energy shared equally be electrons and holes. For single-layer graphene this level is fourfold degenerate, just like all other Landau levels with $|N| \geqslant 1$. In bilayer graphene, the degeneracy of the zero-energy Landau level is eight ($N = 0$ and $|N| = 1$ in Eq. (1)) whereas higher Landau levels ($|N| \geqslant 2$) are again fourfold degenerate. Due to these relativistic Landau-level structures, the well-known integer quantum Hall effect (QHE) [23] observed in conventional two-dimensional electron systems with a parabolic dispersion transforms to a *half-integer* QHE in single-layer graphene [4,5] and to a new type of unconventional integer quantum Hall effect in bilayers [6]. As we will show in more detail in Section 4, the situation can become even more spectacular when increasing the number of layers to three when two different types of quantum Hall effects emerge simultaneously.

3. Magneto-optics on graphene and graphite

It is just the magneto-optical spectroscopy, dealing with excitations from the THz to visible spectral range, which constitutes an important part of high-field research on graphene in LNCMI over the last years. These intense investigations of graphene and other graphene-based systems have been triggered by the seminal work of Sadowski et al. [22], the first optical experiment ever performed on graphene. The observed series of absorption lines in the magneto-transmission spectra of epitaxially grown specimens [24,25] was clearly recognized as intra- and interband excitations in Landau-quantized graphene [26,27]. The Landau level (LL) spectrum with its intriguing $\sqrt{B}$ dependence, previously deduced only from the temperature dependence of magneto-transport data, was thus directly visualized and the Fermi velocity precisely read out, see Fig. 2. The basics of the magneto-optical response of graphene in the quantum regime have thus been established, as was soon after confirmed in experiments on exfoliated specimens in other laboratories [7,28] and further theoretical studies [29,30].

Magneto-optical spectroscopy is nowadays widely applied as a relevant analytic tool, often complementary to transport experiments, to address various phenomena in graphene-based systems. Besides the critical insight into the electronic band structure of individual materials, this techniques serves as a method of choice to investigate elastic and inelastic relaxation processes, electron–phonon coupling or, importantly, also many-body phenomena. A significant part of these intensive investigations of graphene have been carried out at LNCMI [31], often in a broader international collaboration. Let us now present selected areas of this in-house research.
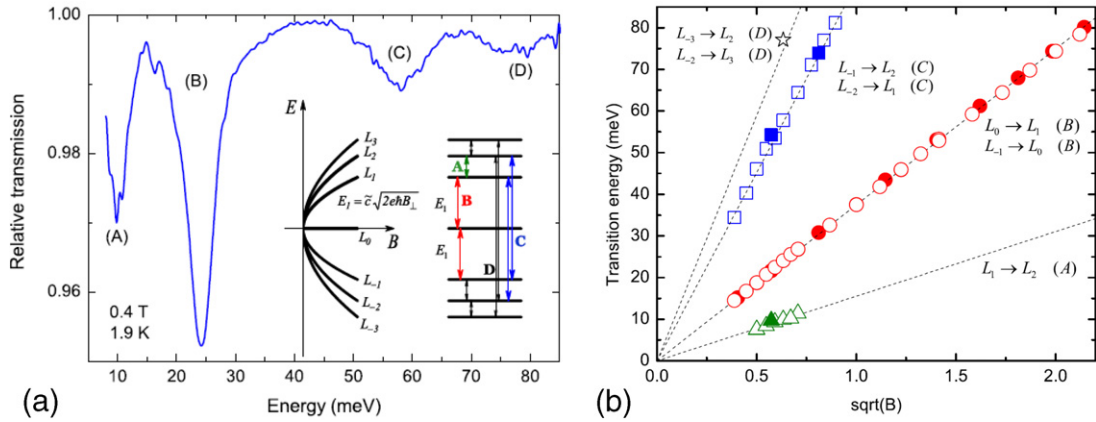
Fig. 2. (a) Typical multi-mode magneto-transmission spectrum of graphene, taken on a few-layer epitaxial specimen (3–5 layers) prepared on C-terminated surface of 4H-SiC [22]. The inset shows a schematic of the evolution of Landau levels with applied magnetic field, and dipole-allowed optical transitions. The transitions occur between two Landau levels $|n|$ and $|n| \pm 1$ where positive and negative n denote electron and hole levels, respectively. (b) Fan chart of observed inter-LL transitions, showing clear $\sqrt{B}$ evolution of all absorption lines. Slope of individual transitions is defined by a single scaling parameter – the Fermi velocity. Reprinted from [22], copyright (2006) by The American Physical Society.
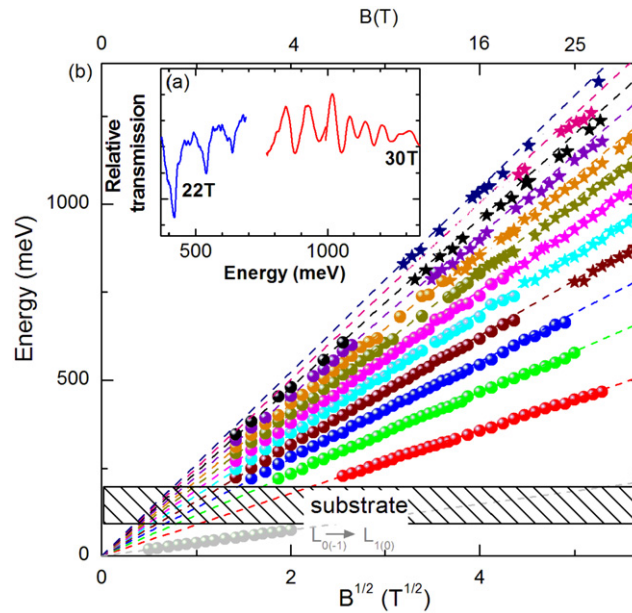

Fig. 3. Energy of the observed optical (inter Landau level) transitions in epitaxial graphene versus the square root of the magnetic field. The observed linear variation of energy versus $\sqrt{B}$ is a direct consequence of the unusual Landau level quantization in graphene. A significant deviation from this dependence is visible only at high magnetic fields and/or high energies. Reprinted from [35], copyright (2008) by The American Physical Society.

3.1. Revealing band structure of graphene-based materials

Tracking the electronic bands in various materials is, from the historical viewpoint, perhaps the most common use of the optical magneto-spectroscopy [32]. This methods enables relatively precise estimates of individual band structure parameters (such as the Fermi velocity in graphene), or optionally, it visualizes the deviations from the proposed band structure model. In LNCMI, this technique has been employed to search for the (possibly non-existing) gap at the Dirac point in various graphene specimens [33,34] and also to quantify the departure of graphene bands from their (ideal) linearity as well as the possible asymmetry of the Dirac cone [35].

To give one characteristic example of such experiments, we focus on the fan chart of interband inter-LL excitations depicted in Fig. 3 in a broad range of energies, from the far- to near-infrared range. Deviations of the electronic bands in graphene from linearity at higher energies, i.e., at larger distances from the Dirac point, is visualized by a clear departure of individual resonances from $\sqrt{B}$ dependence which is typical for ideal 2D massless Dirac fermions. This deviation is mainly caused by the trigonal warping of real electronic bands in graphene, while the effects related to the electron–hole asymmetry have been found negligible. Let us note that the infrared magneto-spectroscopy traced these deviations with a
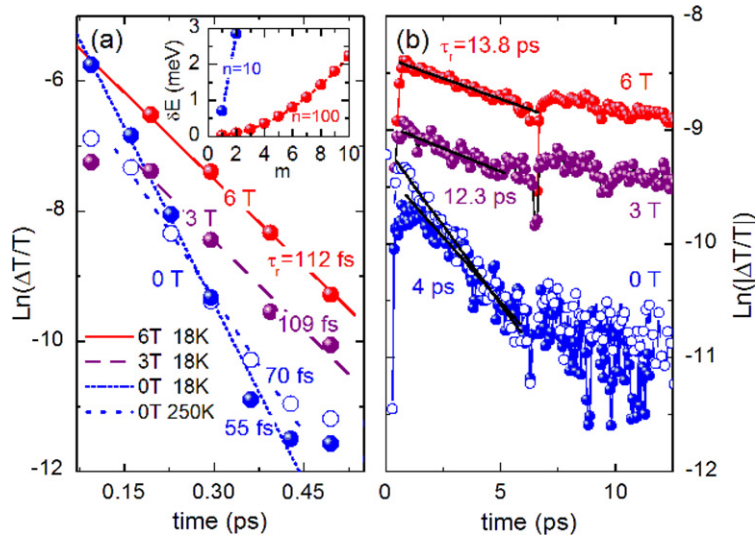
Fig. 4. (a)–(b) Natural log of the differential transmission as a function of a delay between pump and probe pulses measured for magnetic fields (0–6 T) at 18 K. The $B = 0$ T data measured at 250 K is plotted using open circles. The relaxation times τ_r extracted from linear fits are indicated. The inset of (a) shows the calculated energy mismatch for Auger processes for carriers in the $n = 10$ and $n = 100$ Landau level versus change in Landau level index m. Reprinted from [45], copyright (2009) by The American Physical Society.

much higher precision as compared to analogous measurements in zero magnetic field [36,37]. Another successful mission of the infrared magneto-spectroscopy was the identification of well-defined inclusions of (Bernal-stacked) bilayer graphene inside multilayer epitaxial graphene [38], in which the adjacent layers mostly exhibit not Bernal, but rather rotational stacking [39].

3.2. Carrier scattering in graphene

Understanding carrier scattering in graphene, especially the search for intrinsic limits of the carrier mobility and its energy dependence, represents an important direction of work in LNCMI. Using a straightforward method of spotting the Landau quantization at low fields, the infrared/THz magneto-spectroscopy enabled estimates of the carrier mobility in graphene systems, on which transport experiments can hardly be performed. For epitaxial graphene on the carbon-face of SiC, i.e., for a multilayer system with a unique rotational stacking of adjacent layers, the carrier mobility at room temperature exceeds 250 000 cm^2/(V s) [33], a record value among all other solid state materials. The carrier mobility in excess of 10^7 cm^2/(V s) has been reported in analogous experiment, which addressed the decoupled graphene flakes on the surface of natural graphite [34]. Such a high mobility remains an order of magnitude above the best man-made graphene ever fabricated [40]. This represents an important challenge for further developments of current graphene technologies. Recently, the Landau level spectroscopy of interband resonances allowed to find the energy dependence of the relaxation time, $\tau(E)$, and/or mobility in epitaxial graphene [41]. The result, the $\tau(E) \sim |E|^{-1}$ dependence, well corresponds to early predictions for graphene [42,43] but it clearly deviates from behavior typical of exfoliated specimens, see, e.g., Ref. [44], where $\tau(E_F) \sim |E_F|$ is usually found in transport measurements. This points towards an intriguing possibility to prepare a system, the conductivity of which does not depend on the carrier concentration.

Investigations of inelastic channels of the charge carrier relaxation in graphene, using time-resolved experiments, have also been initiated. In cooperation with colleagues at the free-electron laser in Dresden (group of M. Helm, HZD-Dresden-Rossendorf), the relaxation of Dirac fermions, traced in the infrared pump-and-probe experiments, has been found as strongly dependent on the energy of photoexcited carriers. The relaxation rate increases roughly linearly with the energy distance from the Dirac point and it is likely due to (inelastic) scattering on optical phonons [46]. Analogous measurements in the Landau-quantized system may bring even more important results, namely, understanding of the carrier dynamics among well-resolved LLs. This is crucial for the concept of a graphene-based laser, widely tunable by the magnetic field [47], for which an effective creation of the population inversion is an essential issue. Pump-and-probe experiments performed [45] at Warsaw University in the collaboration with LNCMI suggest that crucial condition for this – the suppressed Auger recombination among non-equidistantly spaced LLs – might be fulfilled. To illustrate this work, we present results of a degenerate pump–probe technique in the visible range on multilayer epitaxial graphene in Fig. 4. The differential transmission $\Delta T/T$, measured as a function of the delay between the pump and probe pulses for magnetic fields up to 6 T, is characterized by two time-scales. Especially at low temperatures, the observed decay times increase considerably with the applied magnetic field. This can be for the fast component viewed as a suppression of the electron–electron scattering in the emerging Landau quantization.
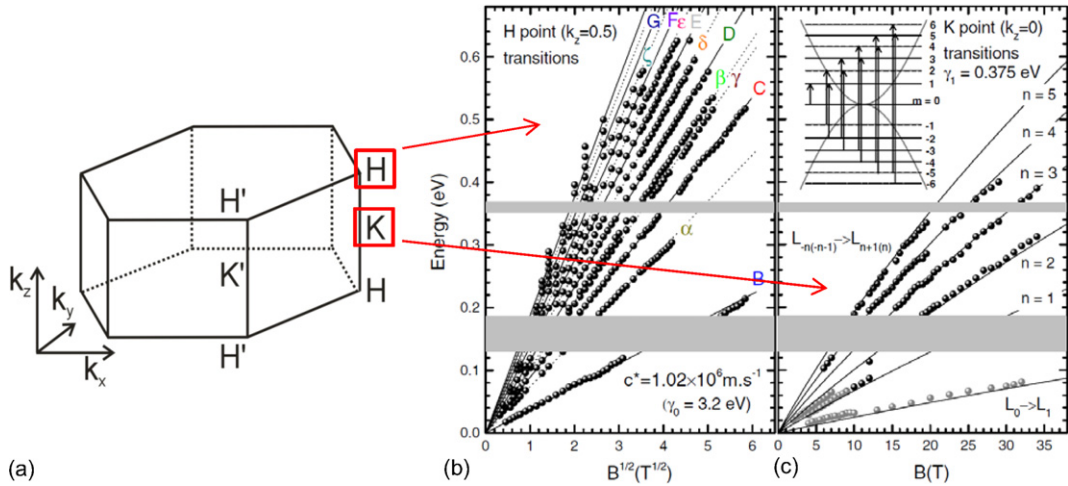
Fig. 5. Part (a): The Brillouin zone of bulk graphite. Dirac-like holes at the *H* point are responsible for a series of the absorption lines in magneto-transmission spectra following a clear $\sqrt{B}$ dependence, see the fan chart in the part (b). Electrons in the vicinity of the *K* point behave as massive Dirac fermions with mass twice enhanced as compared to the truly bilayer graphene and give rise to the magneto-optical response that is linear with *B*, see part (c). Parts (b) and (c) reprinted from [54], copyright (2009) by The American Physical Society.

3.3. Magneto-optical response of bulk graphite

Not only graphene, but also bulk graphite – an "old" material in solid-state physics – has been intensively studied in LNCMI using magneto-optical spectroscopy, a traditional method providing useful insight into the band structure of this material, see, e.g., Refs. [48–50]. At the beginning, the infrared magneto-transmission study of (exfoliated) thin graphite specimens mainly aimed at understanding differences between this Bernal-stacked system and multilayer epitaxial graphene on SiC, with the characteristic rotational stacking [25]. This work finally provided detailed information about the Dirac-like states around the *H* point [51,52] which, by surprise, gives rise to a magneto-optical response very similar to truly graphene [53].

Results of later experiments in high fields led to a simplified picture of the magneto-optical response of bulk graphite: A model imposing an effective mono-layer and bilayer graphene as a substitute for the responses of the *H* and *K* points, respectively, see Fig. 5. This model provides a useful framework for interpretation of subsequent experiments. For instance, it was also the formal similarity of the band structure of bilayer graphene and of the *K* point of graphite, which enabled, using THz magneto-absorption technique, to view bulk graphite as an electronic system in the vicinity of the Lifshitz transition [55]. One deals with the physics analogous to the Lifshitz transition observed recently in truly bilayer graphene [56], but apparently free of the band structure reconstruction due to many-body effects. The effective mono-layer/bilayer model for the response of bulk graphite also served for basic interpretation of the recent high-field high-energy magneto-transmission data taken on natural graphite [57,58]. Nevertheless, rather high complexity of data, see Fig. 6, clearly requires a more elaborated model.

3.4. Raman scattering on graphite and graphene

The Raman technique, so widely used in graphene physics to study phonon-related phenomena, has been in this field at LNCMI first employed to prove the existence of graphene-like bands in epitaxial-grown graphitic multilayer on SiC [59]. In another study at $B = 0$, performed in a close cooperation with the group of A.K. Geim at Manchester University, the thermal conductivity of a self-standing graphene membrane has been deduced [60]. The Raman technique, recently extended to operate in high magnetic fields, became a method alternative to the infrared magneto-spectroscopy. At present the Raman setup at LNCMI can probe excitations down to an energy of about 40 meV (300 cm^{-1}), i.e. it does not probe excitations with energies as low as the infrared technique. However and importantly, it provides the spatial resolution down to microns. This extension made possible the first observation of the magneto-phonon effect in graphene [61–64] proposed (for mono-layer graphene) theoretically [65,66]. The magneto-Raman setup available in LNCMI also enabled observation of the first purely electronic Raman scattering in graphene-based systems, i.e., of the Raman scattering process which does not involve any phonon excitation [67–69]. The observed Raman modes are the inter-LL excitations, see Fig. 7, with selection rules apparently different from the dipole-allowed transitions [70,71]. Soon after, a purely electronic Raman signal at $B = 0$ has also been found in metallic carbon nanotubes at Columbia University [72].
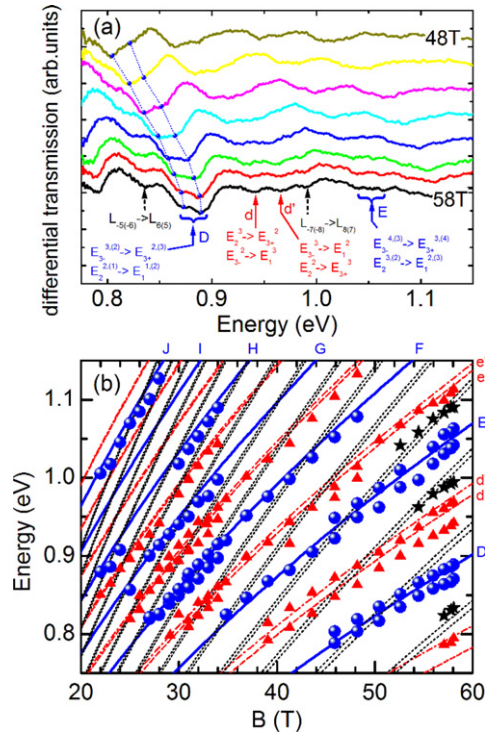
Fig. 6. (a) Typical differential magneto-transmission spectra of natural graphite measured at magnetic fields in the range 48 to 58 T at $T = 4.2$ K. Magnetic field dependence of the observed transitions assigned as follows: H point, graphene series (blue balls), graphite specific series (red triangles); K point (black stars). The lines are calculated energies of the dipole allowed H point (solid, dotted, and, dot-dashed lines) and K point (dashed lines) transitions. Reprinted from [57], copyright (2011) by The American Physical Society.
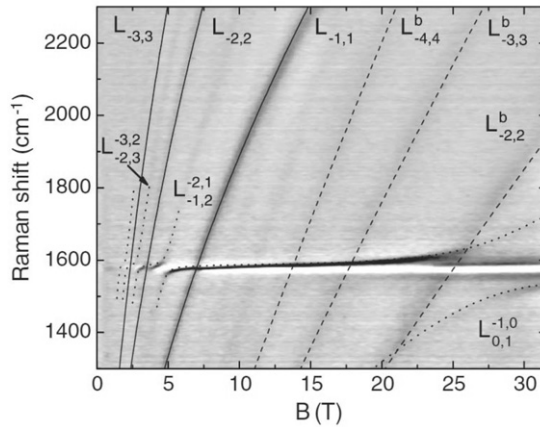
Fig. 7. (False) gray scale plot of magneto-Raman spectra taken on natural graphite specimens. Three different types of excitations are observed: Solid and dotted lines correspond to interband inter-LL excitations in decoupled graphene flakes on graphite. The latter are coupled with E_{2g} phonon line resulting in characteristic avoided crossing behavior [61]. Dashed lines correspond to the interband inter-LL excitations at the K point of bulk graphite, which represent a purely electronic Raman scattering process. Reprinted from [67], copyright (2011) by The American Physical Society.

3.5. Magneto-optical spectroscopy of graphene: Outlook

Investigations of graphene, using method of the optical spectroscopy in magnetic fields, will certainly remain within the main research focus of LNCMI also in future. One clear direction of further work would be entering the field of collective excitations – both in the quantum [22] and classical regime of graphene [73]. Addressing optically graphene in the regime of the fractional quantum Hall effect using magneto-Raman technique is one of ambitious aims. Analogous many-body effects are expected also in the infrared response, which is due to the linearity of graphene bands that violates the Kohn's theorem [74], prohibiting similar phenomena in the cyclotron resonance experiments on conventional materials with parabolic bands. The strength of the Drude weight, enhanced or suppressed as compared to the single-particle estimate [75,76], is

one issue, currently being solved using high-field cyclotron resonance measurements [77]. Concerning the classical collective phenomena, the confined magneto-plasmons are very relevant topic in the current graphene physics. A clear signature of intrinsically confined magneto-plasmons in quasi-free-standing epitaxial graphene have been observed very recently thanks to the collaboration between LNCMI and Université de Genève (I. Crassee and A.B. Kuzmenko) [78]. Notably, graphene-like physics might in future be studied using infrared magneto-spectroscopy also in fully non-carbon system, such as artificial graphene, the investigations of which started recently in LNCMI-G [79].

4. Magneto-transport on graphene-based systems

The magneto-optical experiments described in the previous section constitutes an important technique to address the peculiar energy-level structure of graphene and other carbon-related compounds. Magneto-transport experiments represent an alternative method and are indeed also widely used to investigate the high-field quantum properties of charge carriers. The half-integer quantum Hall effect in graphene [4,5] and the unconventional integer quantum Hall effect in bilayer graphene [6] are prominent examples. Conceptually, this new series of quantum Hall effects can be extended to more than two layers [80], and indeed a first step to trilayer graphene will be shown in the following section.

Another central issue of high-field transport experiments is the possibility of combining size quantization together with the energy spectrum quantization of the charge carriers into Landau levels at high magnetic fields. When the two energy scales of these two effect become comparable, one can investigate and control the energy spectrum of a size quantized system using quantizing magnetic fields. This concept will be applied to graphene nanoribbons and specified in Section 4.2.

4.1. Unconventional quantum Hall effects in graphene

The quantum Hall effect is one of the most remarkable phenomena in condensed matter physics. For a two-dimensional sample, it manifests itself as a zero resistance state as well as quantized values of the Hall resistance under appropriate conditions of temperature, charge density, magnetic field and disorder. It is a direct consequence of the discretization of the energy spectrum of charge carriers (e.g. the Landau levels), which in turns drastically affects the electronic properties of such electron gas. Within a semi-classical framework, the quantum Hall effect is observed when the charge carriers are able to complete full cyclotron orbits in 2D space when the magnetic field is applied perpendicular to the sample's plane. Such a condition is encountered only a low temperature, so that thermal broadening of the Landau levels is weaker than their energetic separation. Also, one would require an excellent mobility of the sample so that diffusion of the electrons onto lattice defects or static impurities do not hinder the full cyclotron orbit of the charge carriers. On the other hand, very high magnetic field can be used as an alternative approach to study disordered two-dimensional systems, and in particular to investigate its impact into the quantum Hall regime. In this section, we will address this question in the case of disordered graphene, by comparing two samples of different mobility. Next, we will extend the discussion to the case of trilayer graphene.

Two graphene flakes were deposited on Si/SiO$_2$ substrate using the micro-mechanical cleavage method [4] and electrically addressed using e-beam lithography-based processes. The SiO$_2$ layer serves as a back-gate in order to change the carrier density in the sample within a range $\Delta n \approx 2 \times 10^{12}$ cm^{-2}. The sample A was mounted in the experimental setup and measured as fabricated whereas sample B was subjected to thermal annealing at 110 °C in vacuum for several hours. As shown in Fig. 8(a), the back-gate voltage required to drive the device at neutrality is $V_g = 52$ V for sample A whereas it reads $V_g = 4$ V only for sample B. The deviations from $V_g = 0$ V of the resistance maximum are linked to charged impurities located at the sample surface or at the interface between graphene and the SiO$_2$ supporting layer. It is difficult to address the nature of such charged impurities: they may result from adsorbed water or molecules present in air or from residue of the fabrication process at the graphene/substrate interface. Nevertheless, the back-gate voltage V_{CNP} corresponding to the system's charge neutrality point (CNP) is an indication of the density and strength of charged impurities influencing the system. Using the model of reference [81], we extract the field effect mobility $\mu = 1300$ cm^2/(V s) for sample A whereas we obtain $\mu = 12\,000$ cm^2/(V s) for sample B. The resistance of these two samples, for which long-range scattering centers (e.g., charged impurities) dominate, are well described by an effective medium theory presented in [82]. In particular, the maximum of resistance (also referred to as the minimum of conductance) is expected to read $R^{max} = 6.46$ kΩ for sample A and $R^{max} = 3.37$ kΩ for sample B, in good agreement with the experimental results (see Fig. 8(a)).

The high field Hall resistance of both samples are reported in Figs. 8(b) and (c). At high carrier density, the systems display clear quantum plateaus at $R_{xy} = \frac{h}{e^2} \cdot \frac{1}{4(n+1/2)}$ with $n = 0, 1, 2, 3, \ldots$ as expected for graphene, where the factor 4 stands for the spin and valley degeneracy. As the carrier density is slightly changed, the Hall resistance curves appear shifted towards lower or higher magnetic field respectively, so that they are identical when plotted as a function of the filling factor $\nu = \frac{n.h}{e.B}$. As the carrier density is further reduced, the low field Hall resistance slope starts to decrease whereas no more quantized plateaus are observed at high field. In this regime the Hall resistance is not well defined and shows strong fluctuations over the full magnetic field range, especially for the dirtier sample (sample A). These trends are consistent with the coexistence of both electron and hole carriers that dominate electronic transport properties, since the Hall coefficient smoothly changes sign when the electron-type carriers start to overcome their hole-like counterparts (and vice-versa) in the close vicinity of the CNP [84]. The resistance fluctuations especially visible for sample A are explained by the presence of local charge density inhomogeneities. It has been shown that charged impurities adsorbed at the graphene surface or located
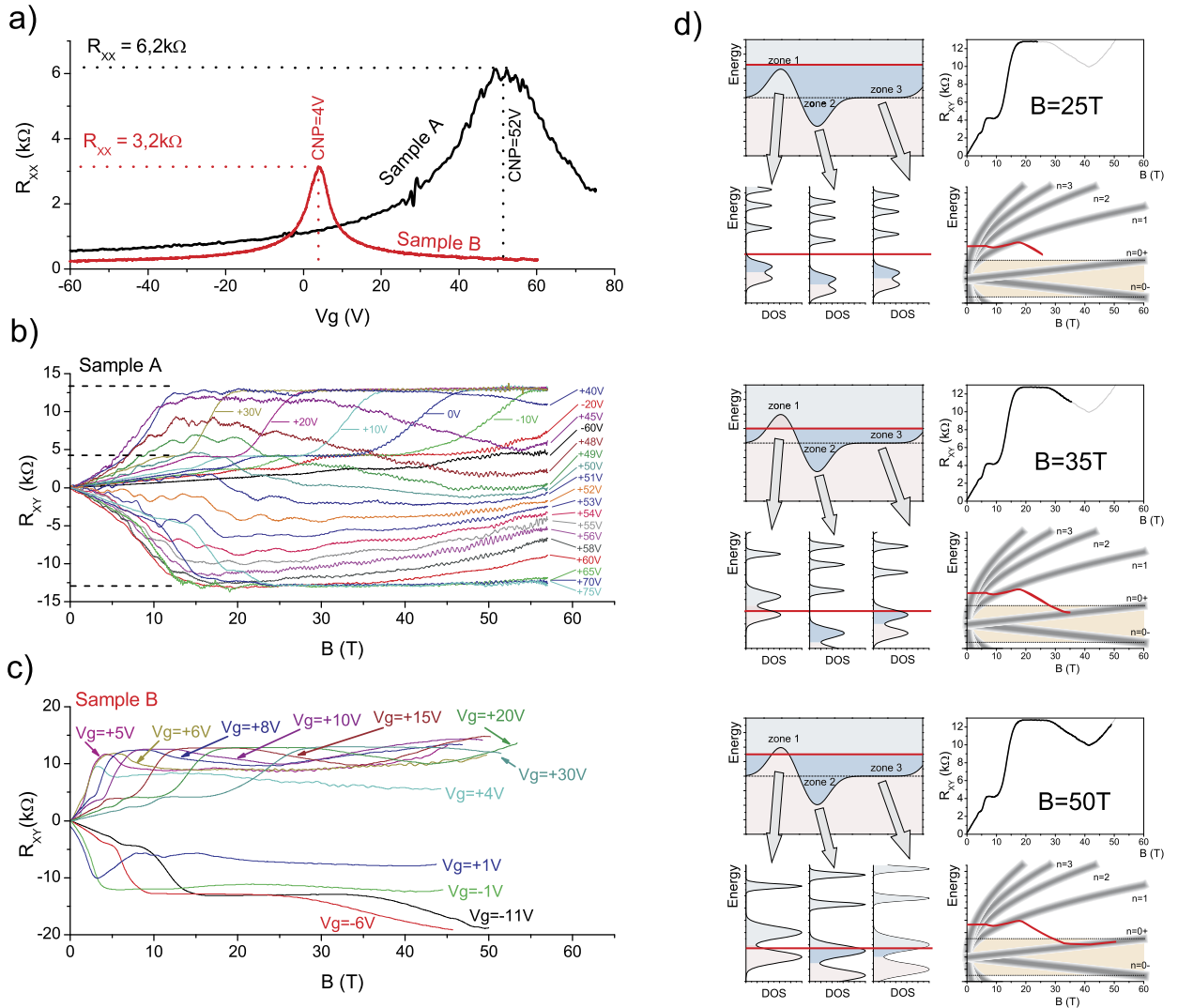
Fig. 8. (a) Resistance of the devices versus gate voltage at zero magnetic field: notice the different back-gate voltages required to reach the CNP as well as the resistance maxima, emphasizing on the different degree of disorder for these two graphene samples. (b) Hall resistance for sample A, for various carrier density across the CNP. (c) Hall resistance for sample B, for different value of the back-gate voltage across the CNP. (d) Three sets of schematic drawings (at different value of the magnetic field) showing the fluctuating potential landscape of disordered graphene (top-left frame), together with the energy distribution of the Landau levels (bottom-left frame). The evolution of the Hall resistance (top-right frame) is put in relation with the Landau levels energy versus magnetic field (as shown in the bottom right frame for zone 3), emphasizing on the Fermi level change when the magnetic field is increased. Adapted from [83].

in the dielectric oxide at short distances from the graphene layer certainly play a dominant role in limiting the mobility of graphene deposited on SiO_2. Such long-range scattering centers create a spatially inhomogeneous screened Coulomb potential in graphene which, in turns, is responsible for the development of electron and hole puddles [85]. The energy and spatial extension of these puddles depend on the density, location and strength of the charged impurities randomly scattered across the sample. The inhomogeneous nature of the sample is irrelevant at high carrier density, but manifest itself as strong fluctuations of the magneto-resistance when the system is driven close to CNP [83,86].

Let us focus on the cleaner sample (sample B) and explain the magnetic field evolution of the Hall resistance. The drawings of Fig. 8(d) represent the system's characteristics for three selected values of the magnetic field, namely $B = 25, 35$ and 50 T. We assume that the Fermi energy is constant all over the sample, but the relative energy of the local neutrality points change from zone to zone thus defining the aforementioned electron and hole puddles. This situation is pictured in the top left inset of Fig. 8(d), which focus on three representative zones of the sample. When the Fermi energy is above the maxima of this fluctuating landscape, electron–electron screening tends to weaken the influence of charged impurities and the system can be considered as homogeneously doped. On the other hand, when the charge carrier concentration is low, some hole puddles naturally appear and the system is inhomogeneous. Depending on the amplitude of the fluctuating

potential, the coexistence of electrons and holes lies within an energy range proportional to ΔV_g. In the lower right panels of Fig. 8(d), such an energy range is represented as an orange-filled area. To ease the discussion, we shall focus on the representative Hall resistance curve at $V_g = +20$ V reproduced in the top-right frames of Fig. 8(d). For intermediate magnetic field (e.g., $B = 20$ T), the Hall resistance lies at $R_{xy} = 12.9$ kΩ at filling factor $\nu = 2$ as expected. Since the Hall resistance is positive and shows a well-defined quantized value for the quantum Hall plateau, one deduces that only hole-type carriers are present in the system and contribute to the Hall resistance. However, for higher magnetic field (e.g., $B = 35$ T), $R_{xy}(B)$ departs from its quantized value and starts to decrease, indicating the presence of negative charge carriers that come into play. Therefore, the magnetic field not only changes the energy spectrum of the system into Landau levels, it also affects the Fermi energy (depicted as the red line in Fig. 8(d)) and opens conduction channels for electrons that were not initially present at low field. Clearly, the "unstable" nature of the R_{xy} plateau at $\pm\frac{1}{2}\frac{h}{e^2}$ is linked to the magnetic-field induced modification of the electron/hole ratio in the presence of charge puddles. For sample A, the scenario would stop at this point since the large LL broadening, together with a large value of ΔV_g, would prevent the observation of any effects related to the LL degeneracy lifting. However, for cleaner samples, the electron–hole coexistence energy range is much reduced and the $n = 0$ LL splitting is sufficient enough to bring the pinned Fermi energy above a threshold value, so that the hole puddles progressively vanish in the system. Therefore the Hall resistance shows an upturn and starts increasing again. Provided magnetic field larger than 55 T could be used, the Hall resistance is likely to establish a plateau at $R_{xy} = h/e^2$ as already observed for high mobility samples.

At this point, it is worth emphasizing on the importance of very high magnetic field when studying disordered graphene samples. Indeed, the quantum Hall regime at low filling factor remains accessible even at fairly high carrier density, thus providing a comprehensive description of the rich high-field magneto-transport phenomena that occur when crossing the Dirac point. As a future prospect, it makes no doubt that studying higher mobility graphene samples in very high magnetic field will be useful to address new electronic states in graphene where electron–electron interactions play a major role. To further illustrate the relevance of high magnetic field, we shall now focus on the integer quantum Hall effect in trilayer graphene.

In trilayer graphene, the zero-energy LL is expected to be 12-fold [88,89] degenerate so that the Hall resistance plateau sequence follows the same ladder as in graphene, but the plateau at $\nu = \pm2$ should be missing. The experimental IQHE in trilayer graphene follows these simple theoretical predictions [90–92], as displayed in Fig. 9(a) together with bi-layer and mono-layer graphene for comparison. These samples have an equivalent carrier density and similar mobility (see legend of Fig. 9 for details). The number of layers for each specimen have been identified using both their Raman signature and the characteristic sequence of QH plateaus. While the bi-layer graphene specimen is easily recognized (with QH plateaus at $R_{xy} = \frac{h}{e^2} \cdot \frac{1}{4.n}$ with n an integer), further analysis is required to distinguish between mono-layer and trilayer graphene. For this purpose, the 2D band feature (also called G' feature) in the Raman scattering spectra are shown in the inset of Fig. 9(a). This band appears in the form of a multicomponent feature characteristic of multilayer graphene [93] in the case of trilayer graphene, in contrast with the one observed for a mono-layer graphene processed in the same way. Thus, the sequence of the Hall resistance plateaus in trilayer graphene is indistinguishable from its mono-layer counterparts except at very high field where the plateau corresponding to $\nu = 2$ is absent. We notice, however, that the Hall resistance slightly overshoots the last $\nu = 6$ resistance plateau. This surprising feature triggered the need for a detailed theoretical analysis of the LL spectrum which goes beyond the simple considerations presented earlier [94,95].

To model the gated trilayer, we employ an SWMC tight-binding parametrization [97,21,98] of the local hopping amplitudes and treat the Coulomb interactions via a self-consistent Hartree approach. There are two possible stacking orders to consider: Bernal (ABA) and rhombohedral (ABC), both illustrated in Fig. 9(b). When a gate voltage is applied to the device, the charge carriers will be distributed among the three layers. Integrating Gauss' law across the layers provides a set of equations which have to be solved self-consistently in order to obtain the trilayer potentials. We include Zeeman splitting, assuming $g = 2$. Finally, some disorder is introduced in the model through a convolution of the density of states with a square distribution of half-width $W_0 = 10$ meV, estimated from the sample's mobility. Fig. 9(c) shows the LL energies and theoretical Hall resistance for both ABC and ABA stacking for gate voltage $V_g = +50$ V, along with the experimental results for R_{xy}. For fields up to 40 T, the measurements agree fairly well with the theoretical predictions for the ABC trilayer, and fail to reproduce the theoretical Hall plateau sequence for the ABA trilayer. The contrasting plateau sequences for ABC and ABA trilayers arise due to the significant differences in their respective Landau level structures. With no bias voltage, the ABC trilayer is inversion symmetric, while the ABA trilayer is not [99]. In the latter case and neglecting Zeeman splitting, quantum Hall steps of amplitude $\Delta G_{xy} = 2.e^2/h$ should be observed for each plateau-to-plateau transition since the LLs originating from valleys K and K' are quite distinct from each other. On the other hand, in the case of ABC stacking, the Landau levels evolve roughly by bunches of four and when disorder effects are taken into account, lead to quantum Hall steps of $\Delta G_{xy} = 4e^2/h$. It is worth noting that the presence of an electric field across the graphene layers (due to the gate voltage induced charge redistributions) breaks the lattice inversion symmetry [100,101]. However, the ABC-stacked LL band-structure is much less affected by electrostatic effects than its ABA-stacked counterpart. Therefore, we have unambiguous determined the rhombohedral stacking order for this particular sample since the main experimental IQHE features are reproduced only for this case. Beyond this assertion, this study also emphasizes on the importance of stacking order in the electronic properties of graphene trilayers. Usually, graphene trilayers deposited on SiO$_2$ show a poor mobility of the order of 1000 cm^2/(V s), justifying the need for very high magnetic fields for IQHE studies.
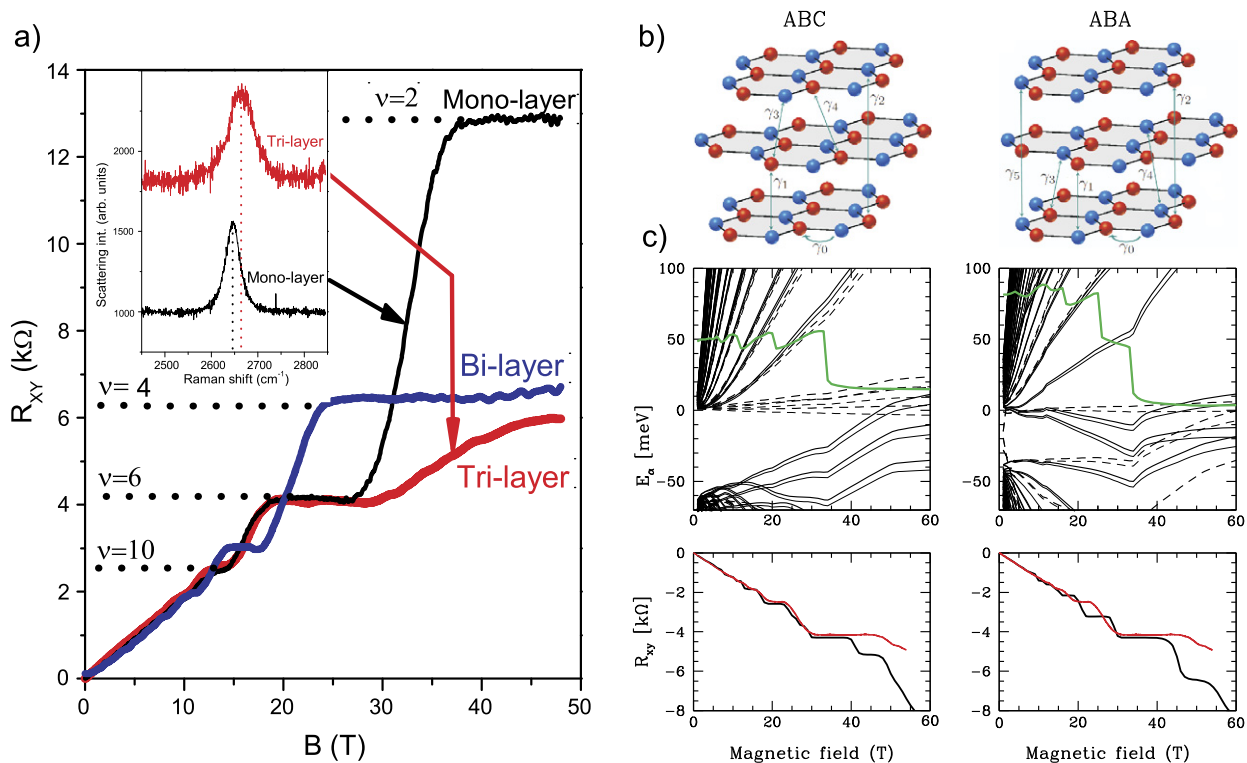
Fig. 9. (a) Quantum Hall effect in mono, bi and trilayer graphene as shown by the black, blue and red curves respectively. These three devices have equivalent carrier density $n = 3.4 \times 10^{12}$ cm^{-2} and similar mobility $\mu = 1200$ cm^2/(V s). Insert: Raman spectrum of trilayer graphene (red curve) and mono-mayer graphene (black curve) measured on the same substrate. (b) Ball-and-stick model for an ABA and ABC-stacked trilayer graphene. (c) Theoretical Landau level structure (top panels) and quantized Hall resistance (bottom panels) using: $V_g = 50$ V, $V_{CNP} = -13.75$ V, $T = 4.2$ K, $W_0 = 10$ meV and $g = 2$. In the top panels, the solid and dashed curves indicate the Landau levels originating from valleys K and K', respectively. In the bottom panels, the experimental and theoretical Hall resistances are displayed by the red and black curves respectively. Reprinted from [87], copyright (2011) by The American Physical Society. (For interpretation of the references to color in this figure, the reader is referred to the web version of this article.)

4.2. Graphene nanoribbons

To benefit from the unusual transport properties of graphene for future carbon-based nano-electronics [102], the fabrication of clean materials has become a central issue. Of great concern is the design of graphene nanoribbons (GNRs), which allow some gap engineering [103]. The transverse confinement leads to 1D electronic sub-bands, whose details depend on width and edge geometry of the ribbons [104]. Experimental evidence of the 1D electronic confinement can be obtained by directly measuring the conductance of a narrow GNR as a function of the electrostatic doping [105,106,96]. In inset of Fig. 10, we present the gate voltage dependent conductance of the 11 nm wide chemical derived GNR [96] under 50 mV bias voltage (V_b), and at various temperatures (from 169 K down to 20 K). Interestingly, a detailed analysis of the $G(V_g)$ curves at 80 K and below unveils reproducible modulations superimposed to the overall increase of the conductance versus the electrostatic doping. These structures become more pronounced at lower bias voltages (Fig. 10 main frame, red and blue curves obtained at 50 and 1 mV, respectively). We assign such conductance profile to the presence of van Hove singularities (vHs), responsible for the enhancement of the backscattering in the diffusive regime. To validate such scenario, extensive tight-binding band-structures calculations are performed on a set of ribbons symmetries with varying widths. Calculations include zigzag (zGNR) and armchair (aGNR) nanoribbons of three types $N = 3m$, $3m + 1$ and $3m + 2$, N being the number of dimer lines. The N values are chosen to explore the full range of the ribbon sample width dispersion (here 11 ± 1 nm), as evaluated by careful AFM analysis. Fig. 10 also shows the density of states $\rho(V_g)$ (dotted-dashed curve) for the armchair configuration of type $3m$ with $N = 90$ corresponding to a nominal width of 10.947 nm which turns out to be the most likely ribbon geometry deduced from the theoretical analysis. Indeed, without any free parameters, an agreement is observed between pronounced modulations of the conductance (local minima or drastic slope changes present on the two $G(V_g)$ curves) and the theoretical sequence of the vHs. Such correspondence is not achieved at all for zGNR and other $3m + 1$ and $3m + 2$ types of aGNR [96]. Note that other N values, multiple of 3, from 87 to 93, in the range of the width uncertainty, also lead to a satisfactory agreement. The energies of the corresponding bands undergo a maximum shift of the order of 6%, which cannot be discriminated on the $G(V_g)$ curves. We conclude that the conductance exhibits 1D sub-bands fingerprints consistent with an armchair arrangement and $3m$ dimer lines (around 90 ± 3) along the GNR width.
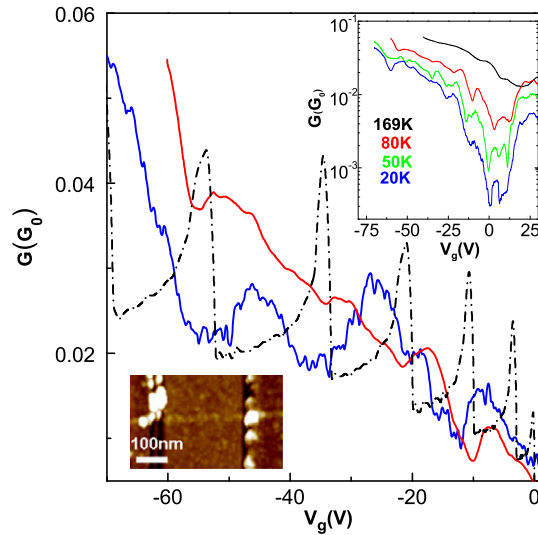
Fig. 10. Conductance versus V_g at 80 K measured on the narrow GNR (width $\simeq$ 11 nm) and for two V_b, 50 mV and 1 mV (respectively red and blue curves). The density of states of a 90-aGNR is superimposed (dashed curve). Top inset: $G(V_g)$ at various temperatures for a wider gate voltage range. Bottom inset: AFM image of the GNR device. Reprinted from [96], copyright (2010) by The American Physical Society. (For interpretation of the references to color in this figure, the reader is referred to the web version of this article.)

In presence of a strong perpendicular magnetic field, anomalous Quantum Hall Effect develops in 2D graphene with unique properties as previously discussed. In nanoribbons, the electronic spectrum is predicted to evolve into magneto-electronic sub-bands resulting from a competition between magnetic and electronic confinement [3,104,108,109]. We recently performed magneto-transport measurements under 60 T on lithographically patterned graphene nanoribbons down to a 70 nm width. The electronic spectrum fragments into an unusual Landau levels pattern [107]. The two-terminal magneto-resistance reveals the onset of magneto-electronic sub-bands, edge currents and quantized Hall conductance. In the following, we present the experimental magneto-resistance (red curves) at different V_g for two GNR of width 100 and 70 nm, Figs. 11(a), (b) and (c)–(e), respectively. In each panel, the black lines correspond to the calculated bottom of the energy bands of armchair ribbons of similar width (100 and 70 nm). At low fields, such minimum energies are always located at $k = 0$. At higher magnetic fields, a set of minima correspond to Landau levels (the flat bands around $k = 0$) and are indicated by continuous lines, which increase as $\sqrt{B}$. The other set of minima (dotted lines) coincide with the minima of the non-degenerate edge region at nonzero-k. This corresponds to the valley degeneracy lifting originating from the electronic confinement in case armchair edge symmetry. The calculated Fermi energy for a given back-gate voltage is plotted in blue. As we can see, the Fermi energy varies with B to accommodate the charges in the available bands and keep the charge density constant. This entails the pinning of the Fermi energy on the bulk Landau levels over large ranges of B, especially for the lowest levels where the corresponding flat bands are more extended. Such a Fermi level pinning together with the valley degeneracy lifting at high fields have important consequences on the magneto-resistance, as the arise of quantum oscillations. At first glance, we see that the maxima of the two terminal resistance develop when the Fermi energy crosses a Landau level (see Ref. [107] for details at low magnetic field). At larger magnetic fields and at larger V_g, the widening of the resistance maxima is a direct consequence of the stronger Fermi energy pinning onto the lowest index Landau levels. Indeed, when crossing the $n = 1$ Landau level, the width of the resistance peak is comparable to the strength of the Fermi energy pinning on this level (see Figs. 11(a) and (b)). In case of the narrowest GNR (see Figs. 11(c)–(e)), we also clearly observe a splitting in two of the resistance maxima when crossing the two $n = 1$ Landau sub-levels at three different back-gate voltages. This unusual feature is assigned to the valley degeneracy lifting driven by an armchair contribution at the edges. It is interesting to note that the armchair contribution at edges is revealed through a magnetic confinement, when the propagating states are strongly pushed to the ribbon edges.

4.3. Magneto-transport on graphene-based materials: Outlook

Magneto-transport technique will in future certainly belong to the most important technique applied to graphene-based materials in LNCMI-G as well as LNCMI-T, to a great extent expanding directions of research discussed above. Namely, a few layer specimens with various stacking (ABA, ABC, ...), perhaps also in a form of nanoribbons. On the other hand, the steadily increasing class of graphene-based systems naturally calls for other high-field experiments – since high-field measurements may overcome, as is often the case, the limited quality of the specimens available. Among these systems, the newest generation of graphene samples, including, e.g., graphene on boron-nitride, with a pronounced fractional quantization in QHE, or even bilayer and multilayer BN/graphene systems, providing novel insight into the Coulomb drag phenomenon, might be of a primary interest for both DC- and pulsed-field facilities in Grenoble and in Toulouse.
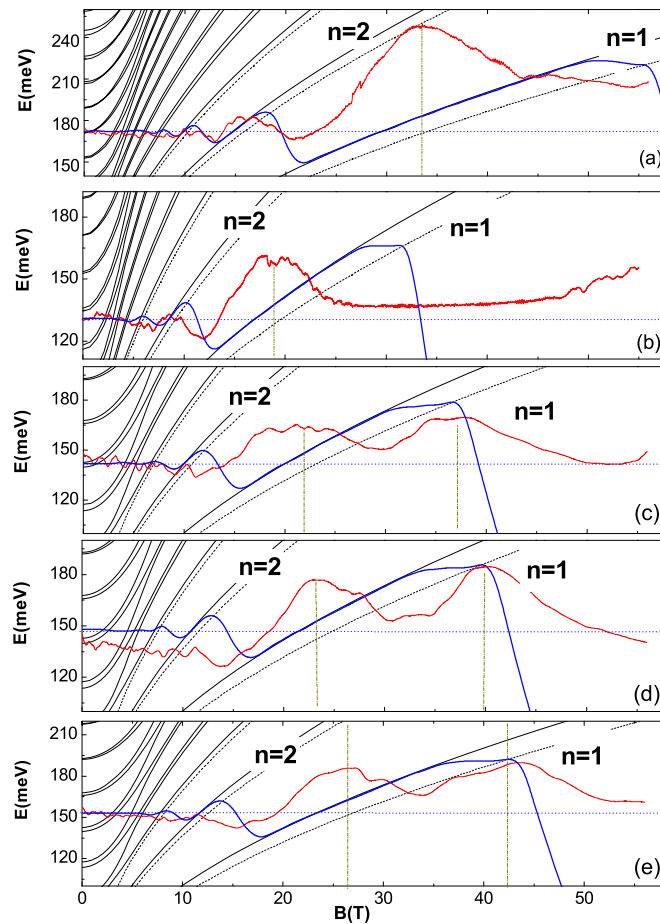
Fig. 11. Simulated magneto-electronic sub-bands versus magnetic field for the 100 nm-wide aGNR (a), (b) and the 70 nm-wide aGNR (c)–(e) directly compared to quantum oscillations at selected V_g. Black lines hold for the edge sub-bands at zero-k. The dashed black lines correspond to the valley degeneracy lifting at nonzero-k. In red are plotted the magneto-resistance curves in arbitrary unit and in blue, the related Fermi energy. Dark yellow vertical lines indicate the resistance peaks shifted to higher magnetic field due to the Fermi energy pinning at low n. Reprinted from [107], copyright (2011) by The American Physical Society. (For interpretation of the references to color in this figure, the reader is referred to the web version of this article.)

5. Summary

We have reviewed recent research activities on graphene-based materials in Laboratoire national des champs magnétiques intenses, CNRS, in Grenoble and Toulouse. Two main experimental techniques – magneto-optical spectroscopy from THz up visible spectral range as well as magneto-transport – have been in recent years been successfully applied to investigate the properties of these new two-dimensional allotropes of carbon and also to revise the properties of bulk graphite. The majority of these experiments have been devoted to establish or verify the band structure character of the investigated materials and they certainly helped to establish and/or to better understand the characteristic nature of massless or massive Dirac electronic states in a number of graphene-based materials.

References

[1] K.S. Novoselov, A.K. Geim, S. Morozov, D. Jiang, M.I. Katsnelson, I. Grigorieva, S. Dubonos, A.A. Firsov, Electric field effect in atomically thin carbon films, Science 306 (2004) 666.
[2] A.K. Geim, K.S. Novoselov, The rise of graphene, Nat. Mater. 6 (2007) 183.
[3] A.H.C. Neto, F. Guinea, N.M.R. Peres, K.S. Novoselov, A.K. Geim, The electronic properties of graphene, Rev. Mod. Phys. 81 (2009) 109.
[4] K.S. Novoselov, A.K. Geim, S.V. Morozov, D. Jiang, M.I. Katsnelson, I.V. Grigorieva, S.V. Dubonos, A.A. Firsov, Two-dimensional gas of massless Dirac fermions in graphene, Nature 438 (2005) 197.
[5] Y.B. Zhang, Y.W. Tan, H.L. Stormer, P. Kim, Experimental observation of the quantum Hall effect and Berry's phase in graphene, Nature 438 (2005) 201.
[6] K.S. Novoselov, E. McCann, S.V. Morozov, V.I. Fal'ko, K.I. Katsnelson, U. Zeitler, D. Jiang, F. Schedin, A.K. Geim, Unconventional quantum Hall effect and Berry's phase of 2π in bilayer graphene, Nat. Phys. 2 (2006) 177.
[7] Z. Jiang, E.A. Henriksen, L.C. Tung, Y.-J. Wang, M.E. Schwartz, M.Y. Han, P. Kim, H.L. Stormer, Infrared spectroscopy of Landau levels of graphene, Phys. Rev. Lett. 98 (2007) 197403.

[8] E.A. Henriksen, Z. Jiang, L. Tung, M.E. Schwartz, M. Takita, Y. Wang, P. Kim, H. Stormer, Cyclotron resonance in bilayer graphene, Phys. Rev. Lett. 100 (2008) 087403.

[9] Z.Q. Li, E.A. Henriksen, Z. Jiang, Z. Hao, M.C. Martin, P. Kim, H.L. Stormer, D.N. Basov, Band structure asymmetry of bilayer graphene revealed by infrared spectroscopy, Phys. Rev. Lett. 102 (2009) 037403.

[10] Y. Zhang, Z. Jiang, J.P. Small, M.S. Purewal, Y.-W. Tan, M. Fazlollahi, J.D. Chudow, J.A. Jaszczak, H.L. Stormer, P. Kim, Landau-level splitting in graphene in high magnetic fields, Phys. Rev. Lett. 96 (2006) 136806.

[11] Z. Jiang, Y. Zhang, H.L. Stormer, P. Kim, Quantum hall states near the charge-neutral Dirac point in graphene, Phys. Rev. Lett. 99 (2007) 106802.

[12] Y. Zhao, P. Cadden-Zimansky, Z. Jiang, P. Kim, Symmetry breaking in the zero-energy Landau level in bilayer graphene, Phys. Rev. Lett. 104 (2010) 066801.

[13] K.S. Novoselov, Z. Jiang, Y. Zhang, S.V. Morozov, H.L. Stormer, U. Zeitler, J.C. Maan, G.S. Boebinger, P. Kim, A.K. Geim, Room-temperature quantum hall effect in graphene, Science 315 (2007) 1379.

[14] A.J.M. Giesbers, U. Zeitler, M.I. Katsnelson, L.A. Ponomarenko, T.M. Mohiuddin, J.C. Maan, Quantum-hall activation gaps in graphene, Phys. Rev. Lett. 99 (2007) 206803.

[15] A.J.M. Giesbers, U. Zeitler, L.A. Ponomarenko, R. Yang, K.S. Novoselov, A.K. Geim, J.C. Maan, Scaling of the quantum hall plateau–plateau transition in graphene, Phys. Rev. B 80 (2009) 241411.

[16] A.J.M. Giesbers, L.A. Ponomarenko, K.S. Novoselov, A.K. Geim, M.I. Katsnelson, J.C. Maan, U. Zeitler, Gap opening in the zeroth Landau level of graphene, Phys. Rev. B 80 (2009) 201403.

[17] U. Zeitler, A. Giesbers, A. McCollam, E. Kurganova, H. van Elferen, J. Maan, High-field electronic properties of graphene, J. Low Temp. Phys. 159 (2010) 238.

[18] C.R. Dean, A.F. Young, P. Cadden-Zimansky, L. Wang, H. Ren, K. Watanabe, T. Taniguchi, P. Kim, J. Hone, K.L. Shepard, Multicomponent fractional quantum hall effect in graphene, Nat. Phys. 7 (2011) 693.

[19] P.R. Wallace, The band theory of graphite, Phys. Rev. 71 (1947) 622.

[20] E. McCann, V.I. Fal'ko, Landau-level degeneracy and quantum hall effect in a graphite bilayer, Phys. Rev. Lett. 96 (2006) 086805.

[21] J.W. McClure, Band structure of graphite and de Haas–van Alphen effect, Phys. Rev. 108 (1957) 612.

[22] M.L. Sadowski, G. Martinez, M. Potemski, C. Berger, W.A. de Heer, Landau level spectroscopy of ultrathin graphite layers, Phys. Rev. Lett. 97 (2006) 266405.

[23] K.v. Klitzing, G. Dorda, M. Pepper, New method for high-accuracy determination of the fine-structure constant based on quantized hall resistance, Phys. Rev. Lett. 45 (1980) 494.

[24] C. Berger, Z. Song, T. Li, X. Li, A.Y. Ogbazghi, R. Feng, Z. Dai, A.N. Marchenkov, E.H. Conrad, P.N. First, W.A. de Heer, Ultrathin epitaxial graphite: 2d electron gas properties and a route toward graphene-based nanoelectronics, J. Phys. Chem. B 108 (2004) 19912.

[25] W.A. de Heer, C. Berger, X. Wu, P.N. First, E.H. Conrad, X. Li, T. Li, M. Sprinkle, J. Hass, M.L. Sadowski, M. Potemski, G. Martinez, Epitaxial graphene, Solid State Commun. 143 (2007) 92.

[26] M.L. Sadowski, G. Martinez, M. Potemski, C. Berger, W.A. de Heer, Magneto-spectroscopy of epitaxial graphene, Int. J. Mod. Phys. B 21 (2007) 1145.

[27] M.L. Sadowski, G. Martinez, M. Potemski, C. Berger, W.A. de Heer, Magnetospectroscopy of epitaxial few-layer graphene, Solid State Commun. 143 (2007) 123.

[28] R.S. Deacon, K.-C. Chuang, R.J. Nicholas, K.S. Novoselov, A.K. Geim, Cyclotron resonance study of the electron and hole velocity in graphene monolayers, Phys. Rev. B 76 (2007) 081406R.

[29] V.P. Gusynin, S.G. Sharapov, J.P. Carbotte, Anomalous absorption line in the magneto-optical response of graphene, Phys. Rev. Lett. 98 (2007) 157402.

[30] D.S.L. Abergel, V.I. Fal'ko, Optical and magneto-optical far-infrared properties of bilayer graphene, Phys. Rev. B 75 (2007) 155430.

[31] M. Orlita, M. Potemski, Dirac electronic states in graphene systems: optical spectroscopy studies, Semicond. Sci. Technol. 25 (2010) 063001.

[32] M.L. Cohen, Cyclotron resonance and quasiparticles, AIP Conf. Proc. 772 (2005) 3.

[33] M. Orlita, C. Faugeras, P. Plochocka, P. Neugebauer, G. Martinez, D.K. Maude, A.-L. Barra, M. Sprinkle, C. Berger, W.A. de Heer, M. Potemski, Approaching the Dirac point in high-mobility multilayer epitaxial graphene, Phys. Rev. Lett. 101 (2008) 267601.

[34] P. Neugebauer, M. Orlita, C. Faugeras, A.-L. Barra, M. Potemski, How perfect can graphene be? Phys. Rev. Lett. 103 (2009) 136403.

[35] P. Plochocka, C. Faugeras, M. Orlita, M.L. Sadowski, G. Martinez, M. Potemski, M.O. Goerbig, J.-N. Fuchs, C. Berger, W.A. de Heer, High-energy limit of massless Dirac fermions in multilayer graphene using magneto-optical transmission spectroscopy, Phys. Rev. Lett. 100 (2008) 087401.

[36] R.R. Nair, P. Blake, A.N. Grigorenko, K.S. Novoselov, T.J. Booth, T. Stauber, N.M.R. Peres, A.K. Geim, Fine structure constant defines visual transparency of graphene, Science 320 (2008) 1308.

[37] K.F. Mak, M.Y. Sfeir, Y. Wu, C.H. Lui, J.A. Misewich, T.F. Heinz, Measurement of the optical conductivity of graphene, Phys. Rev. Lett. 101 (2008) 196405.

[38] M. Orlita, C. Faugeras, J. Borysiuk, J.M. Baranowski, W. Strupiński, M. Sprinkle, C. Berger, W.A. de Heer, D.M. Basko, G. Martinez, M. Potemski, Magneto-optics of bilayer inclusions in multilayered epitaxial graphene on the carbon face of sic, Phys. Rev. B 83 (2011) 125302.

[39] J. Hass, F. Varchon, J.E. Millán-Otoya, M. Sprinkle, N. Sharma, W.A. de Heer, C. Berger, P.N. First, L. Magaud, E.H. Conrad, Why multilayer graphene on 4h-sic(000̄1) behaves like a single sheet of graphene, Phys. Rev. Lett. 100 (2008) 125504.

[40] D.C. Elias, R.V. Gorbachev, A.S. Mayorov, S.V. Morozov, A.A. Zhukov, P. Blake, L.A. Ponomarenko, I.V. Grigorieva, K.S. Novoselov, F. Guinea, A.K. Geim, Dirac cones reshaped by interaction effects in suspended graphene, Nat. Phys. 7 (2012) 701.

[41] M. Orlita, C. Faugeras, R. Grill, A. Wysmolek, W. Strupinski, C. Berger, W.A. de Heer, G. Martinez, M. Potemski, Carrier scattering from dynamical magnetoconductivity in quasineutral epitaxial graphene, Phys. Rev. Lett. 107 (2011) 216603.

[42] N.H. Shon, T. Ando, Quantum transport in two-dimensional graphite system, J. Phys. Soc. Jpn. 67 (1998) 2421.

[43] T. Ando, Y. Zheng, H. Suzuura, Dynamical conductivity and zero-mode anomaly in honeycomb lattices, J. Phys. Soc. Jpn. 71 (2002) 1318.

[44] Y.-W. Tan, Y. Zhang, K. Bolotin, Y. Zhao, S. Adam, E.H. Hwang, S.D. Sarma, H.L. Stormer, P. Kim, Measurement of scattering rate and minimum conductivity in graphene, Phys. Rev. Lett. 99 (2007) 246803.

[45] P. Plochocka, P. Kossacki, A. Golnik, T. Kazimierczuk, C. Berger, W.A. de Heer, M. Potemski, Slowing hot-carrier relaxation in graphene using a magnetic field, Phys. Rev. B 80 (2009) 245415.

[46] S. Winnerl, M. Orlita, P. Plochocka, P. Kossacki, M. Potemski, T. Winzer, E. Malic, A. Knorr, M. Sprinkle, C. Berger, W.A. de Heer, H. Schneider, M. Helm, Carrier relaxation in epitaxial graphene photoexcited near the Dirac point, Phys. Rev. Lett. 107 (2011) 237401.

[47] T. Morimoto, Y. Hatsugai, H. Aoki, Cyclotron radiation and emission in graphene, Phys. Rev. B 78 (2008) 073406.

[48] J.K. Galt, W.A. Yager, H.W. Dail, Cyclotron resonance effects in graphite, Phys. Rev. 103 (1956) 1586.

[49] P.R. Schroeder, M.S. Dresselhaus, A. Javan, Location of electron and hole carriers in graphite from laser magnetoreflection data, Phys. Rev. Lett. 20 (1969) 1292.

[50] W.W. Toy, M.S. Dresselhaus, G. Dresselhaus, Minority carriers in graphite and the h-point magnetoreflection spectra, Phys. Rev. B 15 (1977) 4077.

[51] M. Orlita, C. Faugeras, G. Martinez, D.K. Maude, M.L. Sadowski, M. Potemski, Dirac fermions at the h point of graphite: Magnetotransmission studies, Phys. Rev. Lett. 100 (2008) 136403.

[52] M. Orlita, C. Faugeras, G. Martinez, D.K. Maude, M.L. Sadowski, J.M. Schneider, M. Potemski, Magneto-transmission as a probe of Dirac fermions in bulk graphite, J. Phys.: Condens. Matter 20 (2008) 454223.

[53] M. Orlita, C. Faugeras, G. Martinez, D.K. Maude, J.M. Schneider, M. Sprinkle, C. Berger, W.A. de Heer, M. Potemski, Magneto-transmission of multi-layer epitaxial graphene and bulk graphite: A comparison, Solid State Commun. 149 (2009) 1128.

[54] M. Orlita, C. Faugeras, J.M. Schneider, G. Martinez, D.K. Maude, M. Potemski, Graphite from the viewpoint of Landau level spectroscopy: An effective graphene bilayer and monolayer, Phys. Rev. Lett. 102 (2009) 166401.

[55] M. Orlita, P. Neugebauer, C. Faugeras, A.-L. Barra, M. Potemski, F.M.D. Pellegrino, D.M. Basko, Cyclotron motion in the vicinity of a Lifshitz transition in graphite, Phys. Rev. Lett. 108 (2012) 017602.

[56] A.S. Mayorov, D.C. Elias, M. Mucha-Kruczynski, R.V. Gorbachev, T. Tudorovskiy, A. Zhukov, S.V. Morozov, M.I. Katsnelson, V.I. Fal'ko, A.K. Geim, K.S. Novoselov, Interaction-driven spectrum reconstruction in bilayer graphene, Science 333 (2011) 860.

[57] N. Ubrig, P. Plochocka, P. Kossacki, M. Orlita, D.K. Maude, O. Portugall, G.L.J.A. Rikken, High-field magnetotransmission investigation of natural graphite, Phys. Rev. B 83 (2011) 073401.

[58] P. Plochocka, P.Y. Solane, R.J. Nicholas, J.M. Schneider, B.A. Piot, D.K. Maude, O. Portugall, G.L.J.A. Rikken, Origin of electron–hole asymmetry in graphite and graphene, Phys. Rev. B 85 (2012) 245410.

[59] C. Faugeras, A. Nerrière, M. Potemski, A. Mahmood, E. Dujardin, C. Berger, W.A. de Heer, Few-layer graphene on sic, pyrolitic graphite, and graphene: A Raman scattering study, Appl. Phys. Lett. 92 (2008) 011914.

[60] C. Faugeras, B. Faugeras, M. Orlita, M. Potemski, R.R. Nair, A.K. Geim, Thermal conductivity of graphene in corbino membrane geometry, ACS Nano 4 (2010) 1889.

[61] C. Faugeras, M. Amado, P. Kossacki, M. Orlita, M. Sprinkle, C. Berger, W.A. de Heer, M. Potemski, Tuning the electron–phonon coupling in multilayer graphene with magnetic fields, Phys. Rev. Lett. 103 (2009) 186803.

[62] C. Faugeras, P. Kossacki, D.M. Basko, M. Amado, M. Sprinkle, C. Berger, W.A. de Heer, M. Potemski, Effect of a magnetic field on the two-phonon Raman scattering in graphene, Phys. Rev. B 81 (2010) 155436.

[63] C. Faugeras, P. Kossacki, M. Orlita, M. Potemski, A. Mahmood, D.M. Basko, Probing the band structure of quadri-layer graphene with magneto-phonon resonance, New J. Phys. 14 (2012) 095007.

[64] P. Kossacki, C. Faugeras, M. Kühne, M. Orlita, A. Mahmood, E. Dujardin, R.R. Nair, A.K. Geim, M. Potemski, Circular dichroism of magneto-phonon resonance in doped graphene, Phys. Rev. B 86 (2012) 205431.

[65] T. Ando, Magnetic oscillation of optical phonon in graphene, J. Phys. Soc. Jpn. 76 (2007) 024712.

[66] M.O. Goerbig, J.-N. Fuchs, K. Kechedzhi, V.I. Fal'ko, Filling-factor-dependent magnetophonon resonance in graphene, Phys. Rev. Lett. 99 (2007) 087402.

[67] C. Faugeras, M. Amado, P. Kossacki, M. Orlita, M. Kühne, A.A.L. Nicolet, Y.I. Latyshev, M. Potemski, Magneto-Raman scattering of graphene on graphite: Electronic and phonon excitations, Phys. Rev. Lett. 107 (2011) 036807.

[68] P. Kossacki, C. Faugeras, M. Kühne, M. Orlita, A.A.L. Nicolet, J.M. Schneider, D.M. Basko, Y.I. Latyshev, M. Potemski, Electronic excitations and electron–phonon coupling in bulk graphite through Raman scattering in high magnetic fields, Phys. Rev. B 84 (2011) 235138.

[69] M. Kühne, C. Faugeras, P. Kossacki, A.A.L. Nicolet, M. Orlita, Y.I. Latyshev, M. Potemski, Polarization-resolved magneto-Raman scattering of graphenelike domains on natural graphite, Phys. Rev. B 85 (2012) 195406.

[70] O. Kashuba, V.I. Fal'ko, Signature of electronic excitations in the Raman spectrum of graphene, Phys. Rev. B 80 (2009) 241404.

[71] M. Mucha-Kruczyński, O. Kashuba, V.I. Fal'ko, Spectral features due to inter-Landau-level transitions in the Raman spectrum of bilayer graphene, Phys. Rev. B 82 (2010) 045405.

[72] H. Farhat, S. Berciaud, M. Kalbac, R. Saito, T.F. Heinz, M.S. Dresselhaus, J. Kong, Observation of electronic Raman scattering in metallic carbon nanotubes, Phys. Rev. Lett. 107 (2011) 157401.

[73] A.M. Witowski, M. Orlita, R. Stępniewski, A. Wysmołek, J.M. Baranowski, W. Strupiński, C. Faugeras, G. Martinez, M. Potemski, Quasiclassical cyclotron resonance of Dirac fermions in highly doped graphene, Phys. Rev. B 82 (2010) 165305.

[74] W. Kohn, Cyclotron resonance and de Haas–van Alphen oscillations of an interacting electron gas, Phys. Rev. 123 (1961) 1242.

[75] S.H. Abedinpour, G. Vignale, A. Principi, M. Polini, W.-K. Tse, A.H. MacDonald, Drude weight, plasmon dispersion, and ac conductivity in doped graphene sheets, Phys. Rev. B 84 (2011) 045429.

[76] J. Horng, C.-F. Chen, B. Geng, C. Girit, Y. Zhang, Z. Hao, H.A. Bechtel, M. Martin, A. Zettl, M.F. Crommie, Y.R. Shen, F. Wang, Drude conductivity of Dirac fermions in graphene, Phys. Rev. B 83 (2011) 165113.

[77] M. Orlita, I. Crassee, C. Faugeras, A.B. Kuzmenko, F. Fromm, M. Ostler, T. Seyller, G. Martinez, M. Polini, M. Potemski, Classical to quantum crossover of the cyclotron resonance in graphene: A study of the strength of intraband absorption, New J. Phys. 14 (2012) 095008.

[78] I. Crassee, M. Orlita, M. Potemski, A.L. Walter, M. Ostler, T. Seyller, I. Gaponenko, J. Chen, A.B. Kuzmenko, Intrinsic terahertz plasmons and magneto-plasmons in large scale monolayer graphene, Nano Lett. 12 (2012) 2470.

[79] L. Nádvorník, M. Orlita, N.A. Goncharuk, L. Smrčka, V. Novák, V. Jurka, K. Hruška, Z. Výborný, Z.R. Wasilewski, M. Potemski, K. Výborný, From laterally modulated two-dimensional electron gas towards artificial graphene, New J. Phys. 14 (2012) 053002.

[80] M. Koshino, E. McCann, Landau level spectra and the quantum Hall effect of multilayer graphene, Phys. Rev. B 83 (2011) 165443.

[81] S. Kim, J. Nah, I. Jo, D. Shahrjerdi, L. Colombo, Z. Yao, E. Tutuc, S.K. Banerjee, Realization of a high mobility dual-gated graphene field-effect transistor with Al_2O_3 dielectric, Appl. Phys. Lett. 94 (2009) 062107.

[82] S. Adam, E. Hwang, V. Galitski, S.D. Sarma, A self-consistent theory for graphene transport, P. N. A. S. 104 (2007) 18392.

[83] J.M. Poumirol, W. Escoffier, A. Kumar, M. Goiran, B. Raquet, J. Broto, Electron–hole coexistence in disordered graphene probed by high-field magneto-transport, New J. Phys. 12 (2010) 083006.

[84] J.-M. Poumirol, W. Escoffier, A. Kumar, B. Raquet, M. Goiran, Impact of disorder on the $\nu = 2$ quantum hall plateau in graphene, Phys. Rev. B 82 (2010) 121401.

[85] W. Zhu, V. Perebeinos, M. Freitag, P. Avouris, Carrier scattering, mobilities, and electrostatic potential in monolayer, bilayer, and trilayer graphene, Phys. Rev. B 80 (2009) 235402.

[86] A. Rycerz, J. Tworzydlo, C.W.J. Beenakker, Anomalously large conductance fluctuations in weakly disordered graphene, EPL (Europhys. Lett.) 79 (2007) 57003.

[87] A. Kumar, W. Escoffier, J.M. Poumirol, C. Faugeras, D.P. Arovas, M.M. Fogler, F. Guinea, S. Roche, M. Goiran, B. Raquet, Integer quantum hall effect in trilayer graphene, Phys. Rev. Lett. 107 (2011) 126806.

[88] H. Min, A.H. MacDonald, Chiral decomposition in the electronic structure of graphene multilayers, Phys. Rev. B 77 (2008) 155416.

[89] M. Ezawa, Intrinsic Zeeman effect in graphene, J. Phys. Soc. Jpn. 76 (2007) 094701.

[90] F. Zhang, J. Jung, G.A. Fiete, Q. Niu, A.H. MacDonald, Spontaneous quantum hall states in chirally stacked few-layer graphene systems, Phys. Rev. Lett. 106 (2011) 156801.

[91] T. Taychatanapat, K. Watanabe, T. Taniguchi, P. Jarillo-Herrero, Quantum hall effect and Landau-level crossing of Dirac fermions in trilayer graphene, Nat. Phys. 7 (2011) 621.

[92] L. Zhang, Y. Zhang, J. Camacho, M. Khodas, I. Zaliznyak, The experimental observation of quantum hall effect of $l = 3$ chiral quasiparticles in trilayer graphene, Nat. Phys. 7 (2011) 953.

[93] D. Graf, F. Molitor, K. Ensslin, C. Stampfer, A. Jungen, C. Hierold, L. Wirtz, Raman imaging of graphene, Solid State Commun. 143 (2007) 44.

[94] F. Guinea, A.H. Castro Neto, N.M.R. Peres, Electronic states and Landau levels in graphene stacks, Phys. Rev. B 73 (2006) 245426.

[95] D. Arovas, F. Guinea, Stacking faults, bound states, and quantum hall plateaus in crystalline graphite, Phys. Rev. B 78 (2008) 245416.
[96] J.-M. Poumirol, A. Cresti, S. Roche, W. Escoffier, M. Goiran, X. Wang, X. Li, H. Dai, B. Raquet, Edge magnetotransport fingerprints in disordered graphene nanoribbons, Phys. Rev. B 82 (2010) 041413.
[97] J.C. Slonczewski, P.R. Weiss, Band structure of graphite, Phys. Rev. 109 (1958) 272.
[98] J.W. McClure, Electron energy band structure and electronic properties of rhombohedral graphite, Carbon 7 (1969) 425.
[99] M. Koshino, E. McCann, Parity and valley degeneracy in multilayer graphene, Phys. Rev. B 81 (2010) 115315.
[100] M. Aoki, H. Amawashi, Dependence of band structures on stacking and field in layered graphene, Solid State Commun. 142 (2007) 123.
[101] M. Koshino, Interlayer screening effect in graphene multilayers with aba and abc stacking, Phys. Rev. B 81 (2010) 125304.
[102] F. Schwierz, Graphene transistors, Nat. Nanotechnol. 5 (2010) 487.
[103] M.Y. Han, B. Özyilmaz, Y. Zhang, P. Kim, Energy band-gap engineering of graphene nanoribbons, Phys. Rev. Lett. 98 (2007) 206805.
[104] A. Cresti, N. Nemec, B. Biel, G. Nielber, F. Triozon, G. Cuniberti, S. Roche, Charge transport in disordered graphene-based low dimensional materials, Nano Res. 1 (2008) 361.
[105] Y. Lin, V. Perebeinos, Z. Chen, P. Avouris, Electrical observation of subband formation in graphene nanoribbons, Phys. Rev. B 78 (2008) 161409.
[106] N. Tombros, A. Veligura, J. Junesch, M.H.D. Guimaraes, I.J. Vera-Marun, H.T. Jonkman, B.J. van Wees, Quantized conductance of a suspended graphene nanoconstruction, Nat. Phys. 7 (2011) 697.
[107] R. Ribeiro, J.-M. Poumirol, A. Cresti, W. Escoffier, M. Goiran, J.-M. Broto, S. Roche, B. Raquet, Unveiling the magnetic structure of graphene nanoribbons, Phys. Rev. Lett. 107 (2011) 086601.
[108] K. Wakabayashi, M. Fujita, H. Ajiki, M. Sigrist, Electronic and magnetic properties of nanographite ribbons, Phys. Rev. B 59 (1999) 8271.
[109] K. Wakabayashi, Electronic transport properties of nanographite ribbon junctions, Phys. Rev. B 64 (2001) 125428.